Proceedings of the
4th JSME-KSME Thermal Engineering Conference
October 1-6, 2000, Kobe, Japan

G114

THE SPATIAL AMPLIFICATION OF DISTURBANCES IN VERTICAL NATURAL CONVECTION FLOWS OF WATER NEAR DENSITY EXTREMUM

Young-Kyu Hwang*

* School of Mechanical Engineering, Sungkyunkwan University
300 Chunchun-dong, Jangan-gu, Suwon 440-746, S. Korea
*Professor

ABSTRACT Numerical solutions of the hydrodynamic stability equations for buoyancy-induced flows adjacent to a vertical, planar, isothermal surface in cold pure water have been obtained for various values of the density extremum parameter $R = (T_m-T_\infty)/(T_0-T_\infty)$. The present numerical study yields neutral stability results for the region of the flows corresponding to $0.0 \le R \le 0.1515$, where outside buoyancy force reversals arise. Also, it includes the first stability analysis by obtaining the spatial amplification of disturbances. When the stability results of the present work are compared to the previous experimental data, the numerical results agree well .

Keywords: Neutral Stability, Spatial Amplification, Outside Buoyancy Force Reversal, Density Extremum Parameter

1. INTRODUCTION

The existence of a density extremum near 4°C significantly affects the characteristics of buoyancy induced flows in cold water (Gebhart[1]; Gebhart *et al.*[2]). The occurrence of bi-directional buoyancy forces in the thermal boundary layer complicates their stability analysis. This study is the continuation of Hwang *et al.* [3] to analyze the stability of laminar, vertical natural convection flows in cold pure water in the presence of buoyancy force reversals. In this part, we treat the case of disturbances of downflow, *i. e.*, outside buoyancy force reversals.

Our results are very accurate because the stability equations has been solved using an adequate computing code (COLNEW) designed to accurately solve two point boundary-value problems (Ascher *et al.* [4]; Bader and Ascher [5]). Moreover, our results are new in that we have analyzed the stability by obtaining the spatial amplification contours of disturbances of the steady-state solutions found in this problem by El-Henawy *et al.* [6].

Most of the past stability studies utilize the Boussinesq formulation of the density as a linear function of temperature, such as for flows in air, warm water etc. Recently, Gebhart *et al.* [2] have comprehensively reviewed the literature in this regard.

In the present study, the system under consideration (as seen in Fig.1) is quiescent, cold, pure water adjacent to a vertical, planar, isothermal, impermeable surface. In this situation the Boussinesq approximation does not accurately express the buoyancy force.

This is due to the existence of the density extremum of cold water (its density is maximum at T_m = 4.029325 at 1 bar) in the thermal boundary layer. A considerable buoyancy force reversal arises across the thermal boundary layer. To predict the resulting subtle flow patterns, the following density extremum parameter was defined by Gebhart and Mollendorf [7]

$$R = \frac{T_m - T_\infty}{T_0 - T_\infty} \tag{1}$$

where T_o and T_∞ are temperature of the isothermal surface and the temperature of the ambient medium (cold pure water), respectively.

The analysis of the steady-state flows in the presence of buoyancy force reversals in the range of $0 < R < 0.5$ is complex. To save space we do not discuss these matters in detail here, but we refer to Wilson and Wyas [8], and Carey and Gebhart [9] for experimentally observed flows and to El-Henawy *et al.* [6], Gebhart and Mollendorf [10], and Carey *et al.* [11] for the representation of similarity solutions for such flows.

This study is concerned principally with the

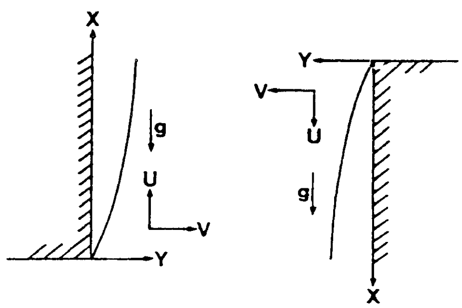

Fig. 1 The coordinate systems.

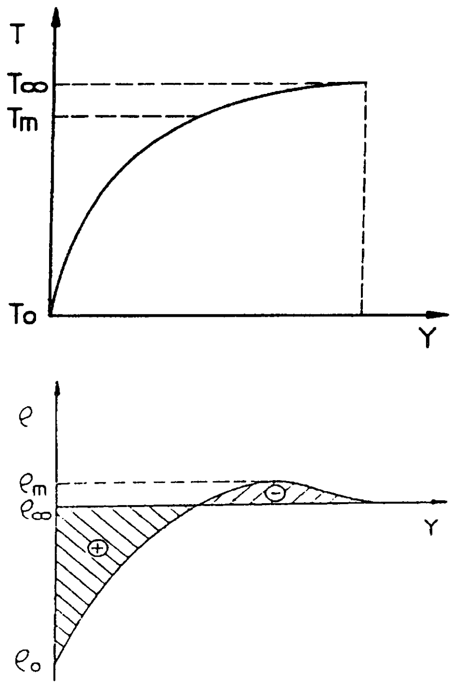

Fig. 2 Illustration of density behavior near T_m ; R =0.1, outside buoyancy force reversal.

presentation, for various values of the density extremum parameter R in the range of $0.0 \le R \le 0.1515$, of numerical results that predict realistic physical conditions of stability for the base flow generated by natural convection adjacent to a vertical, isothermal plate (as seen in Fig. 1) in cold pure water.

The hydrodynamic stability of these base flows is of special interest, since under these conditions outside buoyancy force reversals (such as those seen in Fig. 2) exert a strong influence upon the flow and the multiple steady-state solutions of El-Henawy *et al.* [6] are predicted to exist (see Fig. 3).

The numerical study of the hydrodynamic stability for non-Boussinesq situations is difficult as mentioned by Hwang *et al.* [3]. The difficulty exists partly because the base flow itself is sensitive to buoyancy force reversal via the nonlinear buoyancy-force term in the mathematical model. An additional significant difficulty may come from the presence of a singularity in the linear stability equations as used by Qureshi [12] and Higgins [13]; see also, Higgins and Gebhart [14] and Qureshi and Gebhart [15]. Thus, reformulated stability equations of Hwang *at al.* [3] to be solved is required in order to make them nonsingular.

Due to the difficulties mentioned above, the previous numerical studies were limited to the stability analyses for simple cases of unidirectional buoyancy force: Higgins [13] for several values of R with $1.0 \le R \le 8.0$ and $R = -0.5$ (see also, Higgins and Gebhart [14]); Qureshi [12] for $R = 0$ (see also, Qureshi and Gebhart [15]).

The experimental studies by Higgins and Gebhart [16] and Qureshi and Gebhart [17] in cold water indicate that the density extremum behavior was found to delay transition, compared to results in water at room temperature.

The present numerical study includes neutral stability results for the region of the base flows corresponding to

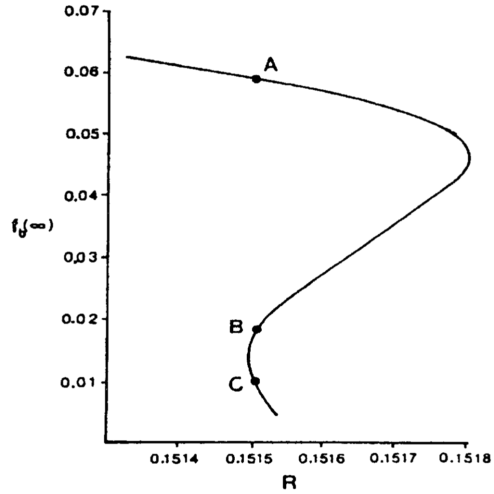

Fig. 3 Detail of the variation of mass-flow rate $f_b(\infty)$ with R . The marks A, B, and C correspond to the three multiple steady-state solutions for the base flow at $R = 0.1515$. From El-Henawy *et al.* [6].

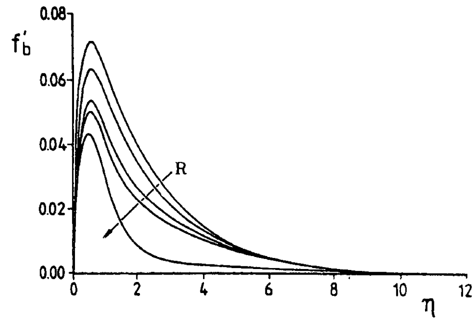

Fig. 4 Distributions of vertical velocity components $f_b'(\eta)$ of the base flows. The arrow indicates increasing $R = 0.0$, 0.05, 0.10, 0.11667 and 0.15.

$0.0 \le R \le 0.1515$ for Pr=11.6. In particular, spatial amplification contours of disturbances are obtained at $R = 0.1167$ and 0.15. Also, neutral stability curves are obtained at R =0.1515 for the three steady-states of the base flow which were found by El-Henawy *et al.* [6]. The effect of outside buoyancy force reversals on stability will be shown.

2. THE GOVERNING EQUATIONS

2.1 Base Flow

The similarity equations for steady laminar base flows (with the coordinate definitions in Fig.1) are well known ; for example, El Henawy *et al.* [6]), Gebhart and Mollendorf [10], and Carey *et al.* [11]. To formulate them the following nondimensional quantities were used : η a similarity variable), $f_b(\eta)$ (stream function), and $\theta_b(\eta)$) (temperature),
where

$$\eta = \frac{yG}{4x},\ \psi_b(x,y) = \nu G f_b(\eta),\ \theta_b(\eta) = \frac{T - T_\infty}{T_0 - T_\infty} \qquad (2a)$$

and

$$G = 4(\frac{1}{4}Gr(x))^{\frac{1}{4}},\ Gr(x) = \frac{gx^3}{\nu^2}\alpha_T\left|T_0 - T_\infty\right|^q \ . \quad (2b)$$

Here α_T and q are the thermal expansion coefficient and exponent, respectively, from the density relation of Gebhart and Mollendorf [7]. For conditions at 1 bar pressure and no salinity, α_T=9.297173$\times$10^{-6} (°C)$^{-q}$ and q=1.894816. The equations for the base flow in similarity form are:

$$f_b \ \ + 3f_b f_b \ \ - 2f_b^{\ 2} + \delta(\left|\theta_b - R\right|^q - \left|R\right|^q) = 0 \quad (3a)$$

$$\theta_b^{''} + 3\,\mathrm{Pr}\, f_b \theta_b^{'} = 0 \quad (3b)$$

with boundary conditions

$$f_b(0) = f_b(0) = f_b(\infty) = \theta_b(0) - 1 = \theta_b(\infty) = 0 \quad (4)$$

with δ = +1 for upward flow, δ = 1 for downward flow; see Gebhart and Mollendorf [10]. Pr = 11.6 is the Prandtl number for cold pure water.

Here we only consider upward flows in the range 0.0 $\le R \le$ 0.1515 where outside buoyancy force reversals occur. The boundary-value problem (3a, b)-(4) was solved on intervals $[0, \eta_\infty]$ with η_∞= 23~300 by using two computer codes: COLNEW (Ascher *et al.* [4]; Bader and Ascher [5]) and BOUNDS (Deuflhard and Bader [18]). Examples of dimensionless vertical velocity profiles for $0 \le R \le$ 0.15 are given in Fig. 4.

Buoyancy force reversals cause significant effects on hydrodynamic transport. As R increases from 0 to 0.15, the downward buoyancy force, near the outer edge of the thermal boundary layer, increases. For multiple steady-states of the base flow, the downward buoyancy force, which becomes stronger, causes an outside flow reversal as R increases from 0.15 to 0.1515.

As R increases from 0 to 0.1333, the location of the single point of inflection in the profiles of the vertical component of velocity shifts closer to the isothermal surface (η=0); see Fig. 4 and Table 1. However, for $0.1333 \le R \le 0.15$, the location of point of inflection remains $\eta_{p,i}$ = 0.97 and does not change significantly as R increases.

The shift of the location of point of inflection associated with its strength $-f_b^{''}(0)$ might increase the limit of stability of flow, just as in forced flow problems. This point will be discussed later.

2.2 The Linear Stability Equation

A linear stability of two dimensional disturbances is considered. The disturbance quantities are normalized in the following manner, where D and U are the characteristic length and velocity:

$$\phi(\eta) = \frac{\overline{\phi}(y)}{UD},\ S(\eta) = \frac{\overline{S}(y)}{T_0 - T_\infty},\ H(\eta) = \frac{\overline{H}(y)}{\rho U^2}$$

$$\alpha = \overline{\alpha}D,\ \beta = \frac{\overline{\beta}D}{U},\ D\frac{4x}{G},\ U = \frac{\nu G^2}{4x} \ . \quad (5)$$

The reformulated stability equations by Hwang *et al.* [3] are used to avoid the singularity in buoyancy force term. The nonsingular Orr-Sommerfeld equations for buoyancy-induced flows are:

x-momentum,

$$(f_b - c)\Phi \ \ - f_B\Phi = -H + \frac{1}{i\alpha G}(\Phi \ \ - \alpha^2\Phi \ \ + Z_0 S) \quad (6a)$$

y-momentum,

$$(f_b - c)\Phi = -\frac{H}{\alpha^2} + \frac{1}{i\alpha G}(\Phi \ \ - \alpha^2\Phi) \quad (6b)$$

energy,

$$(f_b - c)S - \theta_b\Phi = \frac{1}{i\alpha G\ Pr}(S \ \ - \alpha^2 S) \quad (6c)$$

where c = β / α, δ= +1.0 for upflow and δ= 1.0 for down flow, and

$$Z_0 = \delta\frac{(\theta_b - R)}{\left|\theta_b - R\right|}q\left|\theta_b - R\right|^{q-1} \ .$$

The nondimensional boundary conditions for an isothermal vertical surface are:

$$\Phi(0) = \Phi \ (0) = S(0) = \Phi \ (\infty) = S(\infty) = H(\infty) = 0 \ . \quad (7)$$

The linear stability Eqs. (6a-c) and (7) constitute a complex-valued, sixth-order, linear systems of homogeneous differential equations. The eigenvalues of the system are the nondimensional wave number α and frequency β. The ration β / α is referred to as the wave speed c.

As a disturbance of a given frequency is convected downstream, from a position G_1 to G_2, the amplitude ratio e^A for the two location is given by

$$A = -\tfrac{1}{3}\int_{G_1}^{G_2}\alpha_I dG \ . \quad (8)$$

The neutral stability curve is thus $A = 0$ (*i. e.*, $\alpha_I = 0$). The spatial amplification contours are the loci of downstream location have common values of A.

3. NUMERICAL METHOD

To reduce the error propagation and to avoid the inaccuracies in simple shooting of Qureshi [12] and Higgins [13], the two-point-boundary-value-problem solver COLNEW (Ascher *et al.* [4], Bader and Ascher, [5]) was used. With it we were able to compute accurate numerical solutions of the stability equations in the range $0.0 \le R \le 0.1515$. These cannot be found by simple shooting. To generate families of solutions, two different *ad hoc* schemes were used. These are described below. Since there is no way to normalize the solutions of eigenvalue problem (6a-c) and (7) which has all homogeneous boundary conditions, an alternative must be found to avoid the trivial solution.

The first scheme, which succeeded, was to replace the boundary conditions $\Phi'_R(0) = \Phi'_I(0) = 0$ by

$$S'_R(0) = k_1,\ S'_I(0) = -k_2 \tag{9}$$

with $0.25 \le k_1 \le 1.0$ and $0.1 \le k_2 \le 1.0$. For moderate values of α and β, we use $k_1=k_2=1.0$. The computing procedure employed to use the orthogonal collocation code COLNEW for obtaining the neutral stability curve is described below. For a given value G, one guesses a pair of eigenvalues α and β. One then solves the boundary value problem (6a-c) and (7) with the modified boundary conditions (9), replacing $\Phi'_R(0) = \Phi'_I(0) = 0$ using COLNEW, and one iterates by adjusting the values of and until the boundary conditions $\Phi'_R(0) = \Phi'_I(0) = 0$ are satisfied with $|\Phi'_R(0)| = |\Phi'_I(0)| \le 10^{-6}$.

The second scheme is to add the trivial differential equations

$$\alpha' = 0,\ \beta' = 0 \tag{10}$$

to the system (6a-c) and to impose two nonzero conditions $S'_R(0) = -k_1$ and $S'_I(0) = -k_2$ in addition to (7). This scheme yields exact numerical solutions of the original eigenvalue problem (6a-c), (7) and (10). However, to get it to work accurate initial guesses are required.

When we used the first scheme, we insisted that, for a solution to be accepted, the following criteria were all met:

$$\min_{0\le\eta\le\eta_\infty}\left(\frac{|\Phi_R(0)|}{|\Phi_R(\eta)|},\frac{|\Phi_I(0)|}{|\Phi_I(\eta)|}\right) \le 10^{-4} \tag{11a}$$

$$\max\left(\frac{|\Phi_R(0)|}{M},\frac{|\Phi_I(0)|}{M}\right) \le 10^{-7} \tag{11b}$$

where M is the largest magnitude of any of the eigenvector components (i.e., $\Phi, \Phi', \Phi'', S, S', H$) on $0 \le \eta \le \eta_\infty$.
In addition, the error estimates given on output by COLNEW are less than 10^{-4}. The second scheme was used for the purpose of verification and improvement of the numerical results, which were obtained by the first scheme.

4. NUMERICAL RESULTS

Stability results that satisfy the standards for the accuracy Eqs. (11a-b) have been obtained for several values of R in the range $0 \le R \le 0.1515$. In particular, for R = 0.1167 and 0.15, we obtained spatial amplification contour of disturbances. For R = 0.1515, the neutral stability curves for the three steady-states of the flow are computed. These results are presented in Table 1 and Figs. 5-8.

Some of our numerical results on stability are presented in (G, B)-plane,
where

$$B = \beta G^{\frac{1}{3}} = \frac{2\pi f}{\nu}\left(\frac{g}{\nu^2}\alpha_T|T_0 - T_\infty|^q\right)^{-\frac{2}{3}}. \tag{12}$$

This parameter B has no x dependence; it is proportional to the physical frequency f. Constant frequency paths for G are horizontal straight lines in the (G, B)-plane; see Figs. 5-8.

If $|T_o - T_\infty|$ is fixed, a plot or a table in the neutral stability planes is useful in quantitatively analyzing the linear stability results for various values of R, because the parameters G, α, β, and B are depend upon $|T_o - T_\infty|^q$.

The critical Grashof number G_{cr} steadily increases as R increases in the range $0.0 \le R \le 0.1333$, but, interestingly, further increase of R causes G_{cr} to decrease. However, at the same time the value of B^* (*i. e.*, B at G_{cr}) and $B_{\max}$ consistently decrease as R increases; see Table 1 and Figs 5-6. As consequence of these observations, the upper limit of unstable frequencies with respect to R is predicted to be reduced and the flow is more unstable for lower frequencies, as R increases from 0.0 to 0.1515.

It is also observed here that the location of a point of inflection in a base flow has a strong relationship to the critical Grashof number G_{cr}. As R increases from 0 to 0.1333 (and the heat transfer rate $-\theta_b'(0)$ decreases from 1.04697 to 0.8555), the location of the point of inflection $\eta_{p.i}$ in the profile of the velocity of the base flow f_b' shifts from $\eta_{p.i}$=1.163 at R=0 to $\eta_{p.i}$ =0.967 at R= 0.1333; at the same time the stress $-f_b''(\eta_{p.i})$ decreases (see Table 1). In addition, the present results show that the G_{cr} increases from 41.88 at R=0 to 47.69 at R=0.1333. But, as R increases from 0.1333 to 0.15, the $\eta_{p.i}$ increases from 0.967 to 0.971 and the corresponding $-f_b''(\eta_{p.i})$ increases from 0.02925 to 0.03441. Also, G_{cr} decreases from 47.69 at R=0.1333 to 47.39 at R=0.15. As the consequence of the above results, it is found that the shift of $\eta_{p.i}$ to $\eta = 0$ with its weaker stress $-f_b''(\eta_{p.i})$ makes the velocity profile of the base flow more stable.

These phenomena are due to the effect of outside buoyancy force reversals. A slight increase of the

Table 1 Values of $\eta_{p.i}$, $-f_b''(\eta_{p.i})$, B^* and α^* for various values of R.

R	$\eta_{p.i}$	$-f_b''(\eta_{p.i})$	G_{cr}	B^*	α^*
0.0	1.163	0.02847	41.89	0.19536	0.5928
0.05	1.086	0.02575	44.16	0.18027	0.5981
0.10	1.004	0.02574	46.55	0.16188	0.6034
0.11667	0.982	0.02693	47.22	0.15542	0.6081
0.1333	0.967	0.02925	47.69	0.14506	0.5969
0.15	0.971	0.03441	47.39	0.12955	0.5638
0.1515A	-	-	47.17	0.12646	0.5548
0.1515B	-	-	46.98	0.12449	0.5477
0.1515C	-	-	47.01	0.12451	0.5473

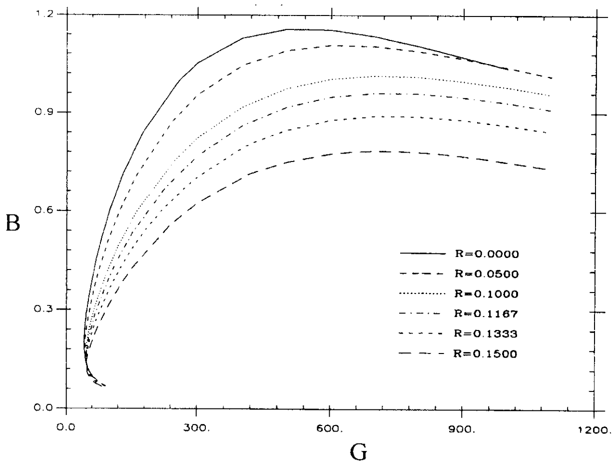

Fig. 5 Computed neutral stability curves in the (G,B) plane.

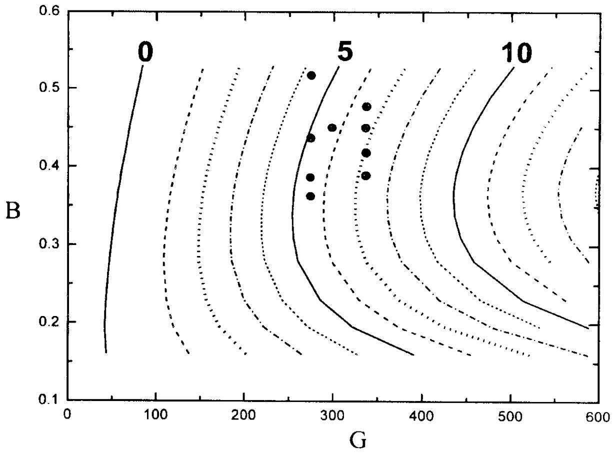

Fig. 7 Spatial amplification contours of disturbances in the (G,B)-plane at R=0.0. ●: Experimental frequency data at R=0.0 come from Higgins[13]

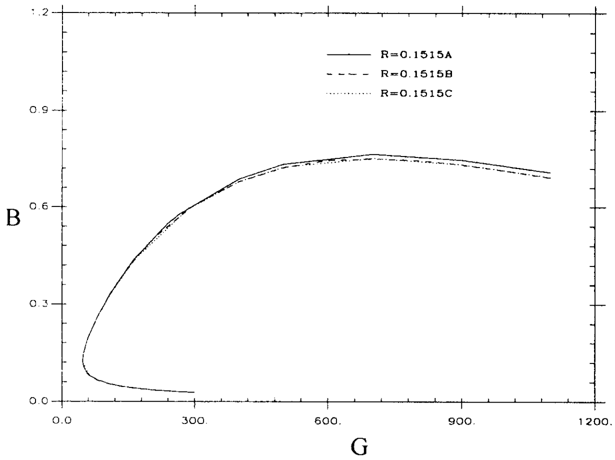

Fig. 6 Computed neutral stability curves in the (G,B) plane for the three steady-states of the base flow at R=0.1515

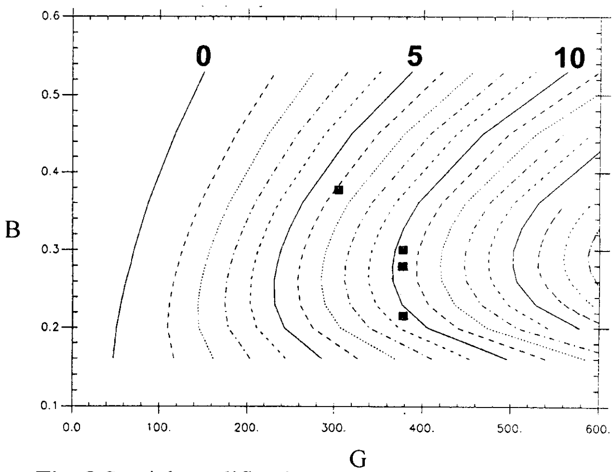

Fig. 8 Spatial amplification contours of disturbances in the (G,B)-plane at R=0.1167. ■:Experimental frequency data at R≈0.12 come from Higgins[13]

downward buoyancy force in the outer region of the thermal boundary layer causes the base flow to be stable, but a further increase of this force causes the base flow to become unstable. Note, while buoyancy force reversals occur for $0<R\leq 0.15$, they are too weak to cause any reversals in the flow.

5. DISCUSSION AND CONCLUSION

The present numerical results indicate that when the parameter R is changed, the characteristic shape of the corresponding neutral stability curve is systematically changed : the critical Grashof number G_{cr} increases for $0< R \leq 0.1333$, but the upper limit of unstable frequency for flows $B_{\max}$ and the quantity B^{*} (i.e., B at G_{cr}) decreases at the same time; see Fig. 5. It is clear from our stability results that the unstable frequency range of disturbances becomes narrower as R increases. In other words, the band of corresponding favored frequency is reduced. Also, the neutral stability curves have blunter noses as R decreases. Not only from the above tendencies but also from the present spatial amplification results in Figs. 7-8, it is found that the corresponding spatial amplification contours have more sharply pointed noses as R increases further toward 0.15. And at the same time we find that the most favored frequency B_f, which is the frequency that, according to theory, amplifies most quickly as the disturbance travels downstream, is decreased from $B_f=0.37$ at R=0.0 and $B_f=0.29$ at R=0.1167 to $B_f=0.23$ at R=0.15. Moreover, the spatial amplification factor A is drastically increased as R increases. For example, for fixed value of G=600, the maximum value of A is near14 at R =0.0, 18 at R =0.1167, and 20 at R=0.15, respectively.

When we compared the spatial amplification results of the present work to the experimental data of Higgins [13] and, also, Higgins and Gebhart [16] at $R\approx 0.0$ and $R\approx 0.12$, the numerical results agree reasonably in a quantitative way with the experimental data. They observed that for $R\approx 0$, the data lie at a frequency slightly higher than the corresponding theoretical frequency B_f=0.37. The range of frequencies, which arose at each G location, is broader than has been observed in warm water. Some intermittent bursts of turbulence were detected at G=378 for

$R \approx 0$. For $R \approx 0.12$, the frequency bands lie closer to, and even below our computed value of $B_f = 0.29$. The band is narrower than that found at $R \approx 0.0$. For $R \approx 0.12$, Higgins [13] (also, Higgins and Gebhart [16]) observed a small amount of burst activity at G=385. From their observation, the point of transition to turbulence occurs some eight or nine times of G_{cr} downstream. Also, their observation implies that the neutral stability curve corresponding to R=0.12 lies left and shifts downward with respect to the neutral stability curve corresponding to R = 0. (See also Table. 1). Higgins and Gebhart also observed that at G=417, the disturbances corresponding to $R \approx 0.12$ were more vigorous than those corresponding to $R \approx 0.0$. They judged that disturbances corresponding to $R \approx 0.12$ are amplified more quickly downstream than those corresponding to $R \approx 0.0$.

From the results of our stability calculation, it is found that there is a stabilizing or destabilizing effect due to the characteristics of the buoyancy force. In the range $0 < R \leq 0.1333$, a small amount of the buoyancy force reversal causes both of the critical Grashof number and of the spatial amplification rate of a disturbance along the most favored frequency to increase significantly. However, in the range $0.1333 < R \leq 0.15$, a further increase of the outside buoyancy force reversal causes the critical Grashof number to decrease. Namely, as R increases, the first instability of the flow occurs later for $0 \leq R \leq 0.1333$, then occurs sooner for $0.1333 < R \leq 0.15$. But, the outside buoyancy force reversal always causes the most favored frequency to be lower and, also, causes the corresponding amplification rate to increase, consistently, as R increases for $0.0 \leq R \leq 0.15$.

At the same time the location of the single point of inflection $\eta_{p,i}$ (in the profile of the velocity of the base flow) and it's stress $-f_b''(\eta_{p,i})$ strongly depend upon the downward buoyancy force (in the outer position of the thermal buoyancy layer) as mentioned in sec 4. Further increase of this force causes an outside flow reversal, which is associated with two points of inflection to exist in the multiple-steady-state-solution region $0.15 < R \leq 0.1518$ found by El-Henawy *et al.*[6], such as the two steady- states of the base flow at R =0.1515 corresponding to the marks B and C in Fig.3. From our results (as seen in Fig. 6 and Table 1), two points of inflection possess slightly lower values of the critical Grashof number than with one. Thus it is predicted that further increase of the downward buoyancy force cause the corresponding flow in the region $0.15 < R \leq 0.1518$ to become slightly unstable.

ACKNOWLEDGEMENT

This work was supported by the Brain Korea 21 Project.

REFERENCES

1. Gebhart, B., Buoyancy induced, motions characteristic of applications in technology, Trans. ASME J. Fluid Eng., Vol. 101(1779), pp. 5-28.
2. Gebhart, B., Jaluria, Y., Mahajan, R. L. and Sammakiea, B., Buoyancy-induced Flows and Transport, (1988), Hemisphere, New York.
3. Hwang, Y., Kazarinoff, N. D. and Mollendorf, J. C., Hydrodynamic stability of multiple steady-states of vertical buoyancy-induced flows in cold pure water, Int. J. Heat Mass Transfer, Vol. 38 (2) (1993), pp. 423-435.
4. Asch, U., Christiansen, J. and Russell, R. D., Collocation software for buoyancy-value ordinary differential equations, ACM Trans., Math software Vol. 7 (1981), pp. 209-222.
5. Bader, G. and Ascher, U., A new basis implementation for a mixed order boundary O.D.E. solver, Tech. Rep. 85-11, (1985), Dept. of Computer Science, University of British Columbia, Vancouver, Canada.
6. El-Henawy, I., Kazarinoff, N., Gebhart, B., Hassard, B. and Mollendorf, J., Numerically computed multiple steady states of vertical buoyancy-induced flows in cold pure water, J. Fluid Mech., Vol. 122 (1982), pp. 235-250.
7. Gebhart, B. and Mollendorf, J. C., A new density relation for pure and saline water, Deep-sea Res. Vol. 24 (1977), pp.831-814.
8. Willson, N. W. and Vyas, B. D., Velocity profile near a vertical ice surface melting into fresh water, Trans. ASME J. Heat Transfer, Vol. 10 (1979), pp. 313-317.
9. Carey, V. P. and Gebhart, B., Visualization of the flow adjacent to a vertical ice surface melting in cold pure water, J. Fluid Mech., Vol. 107 (1981), pp. 37-55.
10. Gebhart, B. and Mollendorf, J. C., Buoyancy-induced flows in water under conditions in which density extremes may arise, J. Fluid Mech., Vol. 89 (1978), pp. 673-707.
11. Carey, V. P., Gebhart, B. and Mollendorf, J.C., Buoyancy force reversals in vertical neutral convection flow in water, J. Fluid Mech., Vol. 97 (1980), pp. 279-297.
12. Qureshi, Z. H., Stability and measurements of fluid and thermal transport in vertical buoyancy induced in cold water, Doctoral dissertation, (1980), SUNYAB, Buffalo, N. Y.
13. Higgins, J. M., stability of buoyancy induced flow of water near the density extremes, adjacent to a vertical, isothermal surface Doctoral dissertation, (1981), SUNYAB, Buffalo, N. Y.
14. Higgins, J. M. and Gebhart, B., The stability of vertical buoyancy induced flow in cold water, Trans. ASME J. Heat Transfer, Vol. 105 (1983), pp. 767-773.
15. Qureshi, Z. H. and Gebhart, B., The stability of vertical thermal buoyancy induced flow in cold pure and saline water, Int. J. Heat Mass Transfer, Vol. 29 (1986), pp. 1838-1392.
16. Higgins, J. M. and Gebhart, B., Measurements of instability and disturbance growth in vertical buoyancy induced flow in cold water, Int. J. Heat Mass Transfer, Vol. 25 (1982), pp. 1379-1409.
17. Qureshi, Z. H. and Gebhart, B., Measurements of fluid and thermal transport in vertical buoyancy induced flows in cold water, Int. J. Heat Mass Transfer, Vol. 24 (1981), pp. 1503-1511.
18. Deuflhard, P. and Bader, G., Multiple shooting techniques revisited, reprint No. 163 (1982), Institut fur Angewnate Math., University of Heidelberg.